01 Mar 2006

Induced-Polarization Measurements on Unconsolidated Sediments from a Site of Active Hydrocarbon Biodegradation

Gamal Z. Abdel Aal

Lee D. Slater

Estella A. Atekwana
Missouri University of Science and Technology, atekwana@mst.edu

Recommended Citation

G. Z. Aal et al., "Induced-Polarization Measurements on Unconsolidated Sediments from a Site of Active Hydrocarbon Biodegradation," *Geophysics*, vol. 71, no. 2, pp. H13-H24, Society of Exploration Geophysicists, Mar 2006.
The definitive version is available at https://doi.org/10.1190/1.2187760

GEOPHYSICS, VOL. 71, NO. 2 (MARCH-APRIL 2006); P. H13–H24, 9 FIGS., 3 TABLES.
10.1190/1.2187760

Induced-polarization measurements on unconsolidated sediments from a site of active hydrocarbon biodegradation

Gamal Z. Abdel Aal[1], Lee D. Slater[2], and Estella A. Atekwana[1]

ABSTRACT

To investigate the potential role that indigenous microorganisms and microbial processes may play in altering low-frequency electrical properties, induced-polarization (IP) measurements in the frequency range of 0.1 to 1000 Hz were acquired from sediment samples retrieved from a site contaminated by hydrocarbon undergoing intrinsic biodegradation. Increased imaginary conductivity and phase were observed for samples from the smear zone (contaminated with residual-phase hydrocarbon), exceeding values obtained for samples contaminated with dissolved-phase hydrocarbons, and in turn, exceeding values obtained for uncontaminated samples. Real conductivity, although generally elevated for samples from the smear zone, did not show a strong correlation with contamination. Controlled experiments on uncontaminated samples from the field site indicate that variations in surface area, electrolytic conductivity, and water content across the site cannot account for the high imaginary conductivity observed within the smear zone.

We suggest that microbial processes may be responsible for the enhanced IP response observed at contaminated locations. Scanning electron microscopy and IP measurements during acid leaching indicate that etched pits on mineral surfaces — caused by the production of organic acids or formed during microbial colonization of these surfaces — are not the cause of the IP enhancement. Rather, we postulate that the accumulation of microbial cells (biofilms) with high surface area at the mineral-electrolyte interface generates the IP response. These findings illustrate the potential use of electrical measurements to noninvasively monitor microbial activity at sites undergoing natural hydrocarbon degradation.

INTRODUCTION

Geochemical and microbiological studies demonstrate that indigenous microorganisms and microbial activity play a role in altering the physicochemical properties of hydrocarbon-contaminated sediments in different ways (Cozzarelli et al., 1994; Cozzarelli et al., 2001). For example, at aged hydrocarbon-contaminated sites, low-molecular-weight organic acids and biosurfactants (surface-active agents) are common microbial metabolic intermediates (Cozzarelli et al., 1995; Cassidy et al., 2001, 2002). The organic acids, when released into solution, increase measured conductivity (a) directly by increasing the electrolyte concentration and (b) indirectly by enhancing the dissolution of minerals, releasing more ions that further increase electrolyte concentration (Cassidy et al., 2001). Biosurfactants produced by microorganisms enhance the solubility and reduce the surface tension of the hydrocarbon fraction sorbed on the mineral grain surfaces by forming micelles (Volkering et al., 1998). As a result, biosurfactants have the tendency to alter the nature of the interface (e.g., wettability) (Ron and Rosenberg, 2001). Furthermore, the bacterial cells themselves have distinct electrical properties that influence subsurface properties (e.g., the effect of attachment-detachment of bacteria on mobility and zeta potential). Such microbial processes are the bases of producing electricity via microbial fuel cells (Park and Zeikus, 2000; Redman et al., 2004). Therefore, it is possible that the induced biophysicochemical changes by micro-organisms, as well as the unique electrical characteristics of bacteria themselves, will have the potential to affect the geophysical properties at aged hydrocarbon-contaminated sites.

There is growing interest in studying the role that microorganisms may play in determining electrical properties in hydrocarbon-contaminated sediments undergoing biodegra-

Manuscript received by the Editor October 27, 2003; revised manuscript received April 11, 2005; published online March 10, 2006.
[1]University of Missouri-Rolla Department of Geological Sciences and Engineering, 1870 Miner Circle, Rolla, Missouri 65409. E-mail: gagv4@umr.edu; atekwana@umr.edu.
[2]Rutgers University, Department of Earth and Environmental Sciences, 101 Warren Street, Rm. 136, Newark, New Jersey 07102. E-mail: lslater@andromeda.rutgers.edu.

dation (Sauck et al., 1998; Sauck, 2000; Werkema et al., 2003; Atekwana, Atekwana, Rowe et al., 2004; Atekwana, Atekwana, Werkema et al., 2004; Atekwana, Werkema et al., 2004). These field and laboratory studies link higher conductivities observed at hydrocarbon-impacted sites to biodegradation processes and changing fluid chemistry. Several ground-penetrating radar (GPR) studies show attenuated reflections probably attributable to the higher electrical conductivity response observed at hydrocarbon-contaminated sites (Bermejo et al., 1997; Bradford, 2003). The self-potential (SP) method has shown possible use as a complementary tool to geochemical measurements to delineate the spatial distribution of in-situ redox potentials associated with microbial degradation of organic contaminant plumes (Naudet et al., 2003).

Recently, we investigated for 36 weeks the induced-polarization (IP) response resulting from biophysicochemical changes of diesel-amended sediments undergoing biodegradation in sand columns at low frequencies (<1000 Hz) (Abdel Aal et al., 2004b). The biotic contaminated column (amended with bacteria) showed temporal increases in electrolytic and interfacial conductivity and temporal decreases in formation factor. These changes were not observed in abiotic columns. Temporal changes in the electrical properties were induced by microbial activity, as verified from observation of temporal changes in the biological and geochemical parameters. A second study investigated the effect of different phases (residual and dissolved) of hydrocarbon on low-frequency electrical properties of unconsolidated sands undergoing biodegradation (Abdel Aal et al., 2004a). This study showed that the relative change in all biogeochemical and electrical parameters was greater (by 10%–30%) in the column contaminated with residual diesel (fraction of hydrocarbon that is adsorbed to soil particles or trapped in soil pores by capillary pressures and does not flow under the influence of gravity or groundwater flow) compared to the column contaminated with dissolved diesel (fraction of hydrocarbon dissolved in water). The greater changes in the electrical parameters were interpreted to result from the relatively higher rate of biodegradation and accompanying biogeochemical alterations at the mineral-fluid interface in the column contaminated with the residual diesel compared to the column contaminated with dissolved diesel (Abdel Aal et al., 2004a).

The IP results obtained in our laboratory indicate that microbial activity induces changes in the interfacial electrical properties of hydrocarbon-contaminated sediments and suggest that IP measurements are potentially valuable in investigating sites of active hydrocarbon biodegradation. This work focuses on whether the effects of biodegradation processes previously observed in laboratory columns are significant enough to be observed at aged hydrocarbon-contaminated sites where the effects of microbial activity presumably are most pronounced. Furthermore, we extend work done by Atekwana, Werkema, et al. (2004); Atekwana, Atekwana, Rowe, et al. (2004); and Werkema et al. (2003) at the same study site using only dc resistivity. From the results of this study, we argue that (a) microbial activity at hydrocarbon-contaminated sites impacts IP measurements and (b) compared with resistivity, IP may be a more diagnostic measure of microbial activity. Our results encourage the use of low-frequency electrical measurements as a tool to complement traditional methods (e.g., groundwater sampling and analysis) in monitoring intrinsic bioremediation of hydrocarbon-impacted sediments and groundwater, with implications for reducing the cost of remediation efforts.

ELECTRICAL PROPERTIES

We measured the frequency-dependent electrical response of soils (0.1–1000 Hz) in the laboratory using an impedance analyzer. Impedance magnitude and phase shift (ϕ) on the sample were recorded relative to a precision reference resistor upon stimulus with a sine-wave current. Results may be presented in terms of magnitude and phase or in terms of real and imaginary components of the impedance. It is a matter of choice whether to present measurements in terms of sample impedance or in terms of resistivity, conductivity, or dielectric permittivity — all calculable from the impedance and sample geometry. Each of these parameters contains a total energy-storage term and a total energy-loss term.

We chose to compute complex conductivity (σ^*). The in-phase (real) conductivity component σ' represents ohmic conduction currents (energy loss), whereas the out-of-phase (imaginary) conductivity component σ'' represents the much smaller (in our frequency range) polarization (energy storage) term. The measured magnitude $|\sigma|$ and phase ϕ parameters are related to the real and imaginary components as follows:

$$|\sigma| = \sqrt{(\sigma'^2 + \sigma''^2)}, \tag{1}$$

$$\phi = \tan^{-1}\left[\frac{\sigma''}{\sigma'}\right] \cong \left[\frac{\sigma''}{\sigma'}\right] \phi < 100\ \text{mRads}. \tag{2}$$

The phase angle measured in IP thus defines the ratio of polarization to conduction. A more detailed explanation of the IP terms used in this section can be found in Lesmes and Frye (2001).

Electric conduction in nonmetallic rocks is ionic, occurring through the pore-filled electrolyte and by ion migration in the electrical double layer forming at the grain-fluid interface. A common assumption is that the electrolytic conductivity σ_{el} and surface conductivity σ'_{surf} add in parallel (Waxman and Smits, 1968; Vinegar and Waxman, 1984):

$$\sigma'(\sigma_w) = \sigma_{el} + \sigma'_{surf} = \left(\frac{1}{F}\right)\sigma_w + \sigma'_{surf}, \tag{3}$$

where σ' is a function of fluid chemistry σ_w and F is the formation factor. The dependence of the surface conductivity on petrophysical parameters is defined elsewhere empirically (Vinegar and Waxman, 1984; Lima and Niwas, 2000) and theoretically (Revil and Glover, 1998).

The relative importance of σ'_{surf} is critically dependent on matrix mineralogy, grain size, degree of saturation, and pore-fluid conductivity. In coarse, clay-free sediments saturated with low-to moderately conductive pore fluids, $\sigma_{el} \gg \sigma'_{surf}$; Archie's (1942) equations can be used to predict σ' as a function of fluid chemistry σ_w, formation factor F, and saturation S_w:

$$\sigma' \cong \sigma_{el} = \frac{1}{F}\sigma_w S_w^n = \sigma'_{sat} S_w^n, \tag{4}$$

where σ'_{sat} is the saturated real conductivity and n is the saturation exponent related to the distribution of fluid within the

pore space. The saturation exponent is a function of the range of saturation studied and the saturation history (Longeron et al., 1989; Knight, 1991). Laboratory studies using unsaturated unconsolidated sediments show that polarization and conduction at low frequencies (<1000 Hz) exhibit power-law dependency on saturation with a smaller exponent for σ'' (polarization) magnitude compared to σ' (conduction) magnitude (Ulrich and Slater, 2004).

Conduction and polarization at the grain-fluid interface are a function of surface area, surface-charge density, surface-ionic mobility, and interfacial geometry (Schön, 1996; Revil and Glover, 1998; Lesmes and Frye, 2001). The IP measurements in unconsolidated sediments and sandstone show a near-linear correlation with surface area (Börner and Schön, 1991; Schön, 1996) and an inverse correlation with grain size (Schön, 1996; Slater and Lesmes, 2002a; Slater and Glaser, 2003). Laboratory studies show that electrolyte chemistry also influences conduction and polarization at the grain-fluid interface (Vinegar and Waxman, 1984; Revil and Glover, 1998; Lesmes and Frye, 2001). Increasing electrolyte concentration generally increases surface-charge density and decreases surface-ionic mobility (Lesmes and Frye, 2001). These are usually second-order effects when considering the relatively limited range of electrolyte concentration encountered in most natural sediments (Slater and Lesmes, 2002b).

SITE HISTORY AND BACKGROUND

Sediments used in this study were retrieved from a site adjacent to an abandoned refinery with a 50-year hydrocarbon spill history located in Carson City, Michigan (Figure 1). Detailed descriptions of the study site can be found in Atekwana, Werkema, et al. (2004). The study area is characterized by glacial deposits consisting of 4.5–6.1 m of fine to medium sands, coarsening at and below the water table to gravel and underlain by a 0.6- to 3.1-m-thick clay unit. The mineralogy of the sediments is predominantly quartz with minor amounts of feldspars, calcite, gypsum, and dolomite. Because of topographic variations at the site, depth to groundwater varies from approximately 1–4 m. Continuous hydrocarbon releases (mostly JP4 jet fuel and diesel) from storage facilities and pipelines have resulted in petroleum hydrocarbons seeping into the subsurface, impacting near-surface sediments and groundwater. Concentrations of benzene, toluene, ethylbenzene, and xylene (BTEX) range from 0.76–481 mg/l in the contaminated plume (Legall, 2002). Hydrocarbon contamination at this site occurs in residual, free (mobile or free liquids moving down through the unsaturated zone independent of the direction of flow of groundwater or surface water), and dissolved product phases. Although no chemical analysis was conducted within the upper part of the vadose zone of contaminated locations, a hydrocarbon vapor phase may exist from the residual phase below, as observed in previous studies (Pasteris et al., 2002). Seasonal water table fluctuation (~0.9 m annually) across the site enhances adsorption of free hydrocarbons (floating on the water table) on the aquifer solids, resulting in a smear zone (dominated by free and residual hydrocarbon contamination) with variable thickness. This smear zone can be divided into lower and upper parts located below and above the mean water table elevation, respectively (Werkema et al., 2003).

Previous geophysical investigations conducted at the site indicate that contaminated locations (free and residual hydrocarbon) within the smear zone have higher bulk conductivity than uncontaminated locations (Werkema et al., 2003; Atekwana, Werkema, et al., 2004). Intrinsic bioremediation is occurring at the site with methanogenesis as the dominant redox process within the core of the plume, while sulfate, iron, and manganese reduction occur at the fringes of the plume (Legall, 2002). Volatile organic acids and biosurfactants have been measured in contaminated groundwater at this site (Cassidy et al., 2002). Microbial studies conducted on sediments and groundwater have documented microorganisms capable of degrading hydrocarbon and have shown that oil-degrading microorganisms make up a large percentage of the heterotrophic microbial population within the hydrocarbon-impacted zones (Atekwana, Werkema, et al., 2004). Table 1 shows some of the geochemical parameters measured for groundwater samples from the site (VRP9, VRP5, and VRP1) during spring when the water table is slightly higher. The data show depletion in terminal electron acceptors (nitrate and sulfate) at contaminated locations VRP5 and VRP1, consistent with biodegradation of the hydrocarbons (Baker and Herson, 1994; Cozzarelli et al., 2001). Enrichment of calcium and silicon ions provides evidence for enhanced mineral weathering, increasing the fluid conductivity at contaminated locations. From Table 1, we conclude that active microbial degradation of hydrocarbon is occurring at contaminated locations.

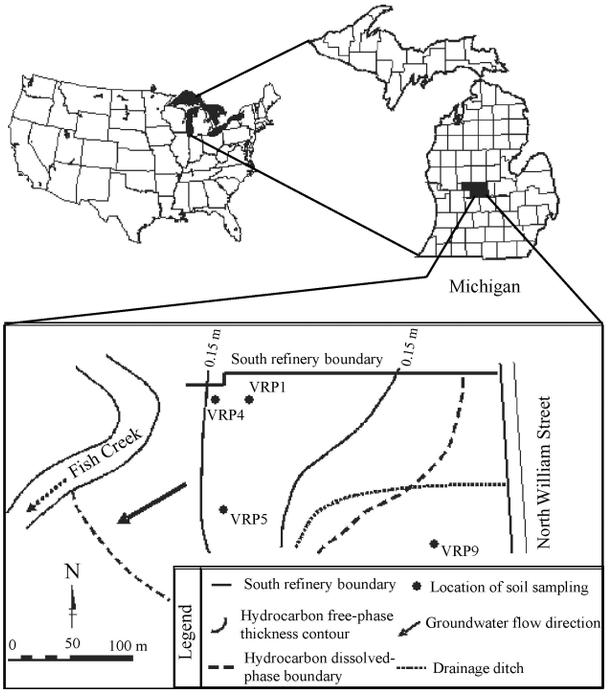

Figure 1. Map of the study area showing the sampling locations (VRP9, VRP5, VRP4, and VRP1) and hydrocarbon distribution in groundwater.

Sediment sampling and characterization

Sediment samples were collected from both uncontaminated and contaminated locations at the study site (Figure 1). Samples were obtained using a Geoprobe rig and were collected in a clear, modified polyethylene terephthalate glycol (PETG) macrocore liner casing, capped and stored upright at 4°C during transportation to the laboratory. To minimize altering of the initial chemical properties of the samples from chemical or biological reactions, we stored the samples in the laboratory at 4°C in a refrigerator until IP measurements were made. Figure 2 shows a schematic of the subsurface, including grain-size distribution, contaminant phase, average depth to the water table, location of measured samples, and smear zones. The grain-size distribution of the sediments was determined at 0.30-m depth intervals by dry sieve analysis. Based on the unified soil-classification system (USCS) (American Society for Testing and Materials, 2000), the composition of the measured samples varies from 0–8% silt and clay (<0.074 mm), 48%–99% sand (4.75–0.074 mm), and 0–5% gravel (>4.75 mm). The residual and free phases of hydrocarbon were determined through visual identification of the sediment samples for the hydrocarbon-stained soil particles and presence of free product, respectively. The dissolved phase of hydrocarbon was previously determined at the study site by Legall (2002). SEM analysis was conducted on five samples (VRP9A, VRP9C, VRP4B, VRP4D, and VRP1B; Figure 2) after air drying at room temperature for a week to investigate any changes in mineral surfaces (e.g., etching or pitting) that might be related to microbial activity. Measurements were acquired with a JEOL JSM-T330A scanning microscope, and images were acquired using Revolution 1.4.7 software at 750× magnification. To investigate changes in surface area related to microbial activity, specific surface-area measurements (m^2/g) were made on the same five samples using the nitrogen Brunauer, Emmett, and Teller (BET) adsorption method (Brunauer et al., 1938). Each sample was measured in triplicate with a NOVA 3200 series surface area analyzer. Porosity of these samples was obtained using a gravimetric method, and the surface area-pore volume ratio (S_{por}) was calculated.

Table 1. Fluid conductivity, nitrate, sulfate, calcium, and silicon in groundwater from multilevel piezometers at the Carson City, Michigan, site.[3]

Sample location	Depth (m)	Fluid conductivity (S/m)	Nitrate (mg/l)	Sulfate (mg/l)	Calcium (mg/l)	Silicon (mg/l)
VRP9	2.27	0.0470	5.6	18.9	62.2	8.0
	2.72	0.0772	5.8	40.5	29.2	9.0
	3.20	0.0852	2.0	44.4	39.5	11.0
	3.49	0.0875	2.0	45.4	41.2	11.0
VRP5	2.25	0.0185	33.1	ND[4]	20.2	14.0
	2.71	0.0318	0.1	1.6	103.9	13.0
	3.16	0.0931	1.1	ND	189.7	20.0
	3.61	0.0891	0.9	ND	153.1	20.0
	4.09	0.0885	ND	2.0	151.5	21.0
VRP1	3.57	0.0815	0.2	10.5	170.5	18.0
	4.02	0.0916	ND	3.8	184.6	16.0
	4.47	0.0944	ND	ND	177.4	15.0
	4.92	0.0946	ND	ND	177.0	16.0
	5.38	0.0943	ND	ND	177.1	15.0
	5.83	0.0957	ND	ND	174.1	17.0
	6.28	0.0935	0.2	ND	141.7	22.0

[3]All data are from measurements below the saturated zone (modified after Legall, 2002). Depletion in terminal-electron acceptors (e.g., NO_3 and SO_4) at contaminated locations VRP1 and VRP5 provide evidence of hydrocarbon degradation; enrichment of ions (e.g., calcium, silicon) provides evidence for enhanced mineral weathering, increasing the fluid conductivity at the contaminated locations VRP1 and VRP5 compared to the uncontaminated location VRP9.

[4]ND — (not detected).

ELECTRICAL MEASUREMENTS

Electrical measurements were made on the soil samples obtained from the field.

Sediment samples from the field

Electrical measurements were obtained with a National Instruments NI 4551 four-electrode dynamic signal analyzer (Slater and Lesmes, 2002a). Phase shift between current sti-

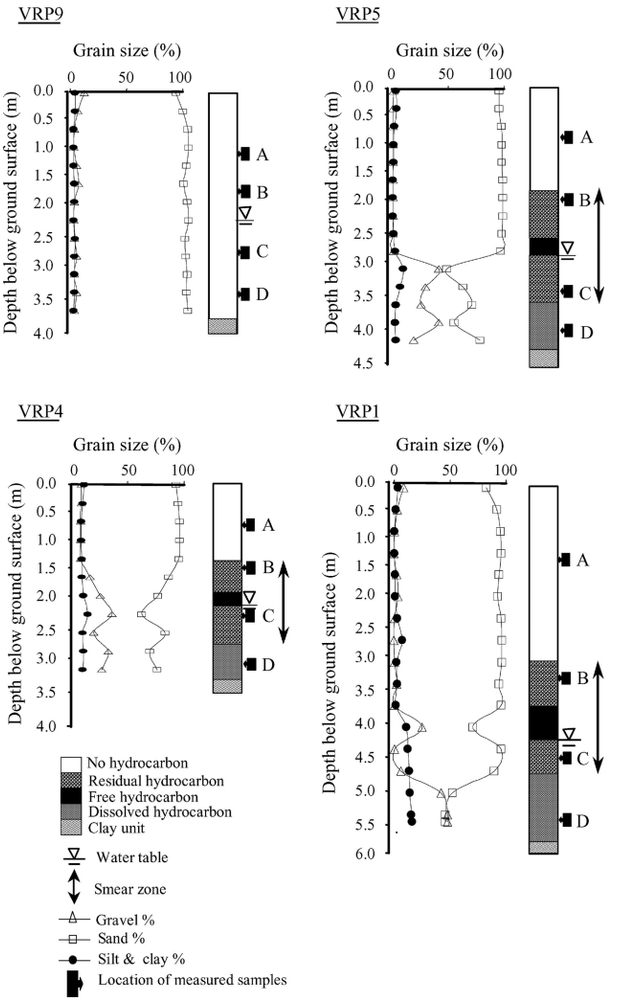

Figure 2. Column schematic showing depths where sediment cores were obtained, contaminant phases, smear zone, grain-size distribution, and mean water depth.

mulus-voltage signal and impedance magnitude was measured at 40 frequencies, spaced at equal logarithmic intervals between 0.1 and 1000 Hz. Current was injected at silver coil electrodes located at sample ends. Sample voltage was measured using silver-silver chloride electrodes located just outside the current flow path. An AD620 preamplifier boosted the input impedance on the voltage channel and prevented current leakage into the circuitry. The phase response of the preamplifier, dependent on frequency and sample resistance, was removed by calibrating a water sample (for which the theoretical phase can be calculated) matching the sample resistance. Repeatability tests indicate that errors are generally less than 0.5 mRad for the phase and 0.5% for impedance magnitude, respectively.

IP measurements on sediments from the field site were made on 16, approximately 20-cm-long, samples (Figure 2) with an internal diameter of 4.3 cm. Each sample was measured intact in the clear PETG macrocore liner casing. The samples represent an uncontaminated background location (VRP9) and locations with residual and dissolved-phase hydrocarbon (VRP5, VRP4, and VRP1; Figure 2). Measurements were also made from samples obtained from the vadose zone, immediately above residual contamination zones (VRP5A, VRP4A, and VRP1A) where vapor-phase contamination is suspected.

Control experiments

Variations in lithology (Figure 2), fluid chemistry (Table 1), and water content (Figure 2) modify electrical properties between samples. Thus, we performed control experiments to constrain the variability in the electrical properties (both the real and imaginary parts) of our samples that could be independent of the effects of contamination and associated microbial degradation. Fluid conductivity and moisture content effects were investigated for uncontaminated sediment samples collected at about 0.30 m below the ground surface from VRP9 (uncontaminated location). The vadose-zone lithology is nearly identical at all locations consisting primarily of sands (~80%–97%) (Figure 2). To test the effect of σ_w on electrical measurements, we progressively saturated the sample with a synthetic groundwater whose σ_w ranged from 0.005–0.140 S/m, spanning the range of σ_w at the field site (0.02–0.1 S/m) (Table 1). Another sample from the same location was used to constrain the dependence of the electrical measurements on S_w. This sample was saturated with 0.01 M sodium chloride (NaCl) solution and then dried by evaporation, with IP measurements obtained at six intervals over the saturation range 34%–98%. The degree of saturation was calculated by measuring the weight reduction associated with evaporation. Measurements were terminated at 34% saturation as a result of excessive contact resistance developing at the current electrodes.

Grain-surface dissolution by organic acids is postulated to be the primary mechanism causing the elevated σ_w observed at hydrocarbon-contaminated sites undergoing active microbial activity (Sauck, 2000). To examine the potential effect of this process on specific surface area and IP response, we washed sediments from the study site (mostly sands) several times with distilled water, dried them at room temperature, and divided the sediments into five subsamples. The mineral-etching procedure of Berner and Holdren (1977) was then used to etch the samples. Four subsamples were treated with 5% hydrofluoric acid and 1% sulfuric acid (H_2SO_4) at 20-minute intervals. The fifth subsample was not subjected to acid treatment and was used as the control sample. The treated samples were washed several times with 1% H_2SO_4 and distilled water to remove any precipitates on the mineral surfaces. All samples were saturated with a sodium-chloride brine solution of 0.012 S/m, and IP measurements in the 0.1–1000-Hz frequency range were obtained. SEM analysis and BET specific surface area measurements of these samples were obtained using the procedures described previously.

RESULTS

The results of the measured IP parameters are presented below.

Sediment samples from the field

Figure 3 shows σ', σ'', and ϕ obtained for samples from the saturated zone. The uncontaminated samples are plotted using filled symbols; contaminated samples (residual and dissolved hydrocarbon) are plotted with open symbols. The σ' magnitude for all samples is to the first-order constant between 0.1 and 1000 Hz (Figure 3a). Samples from the uncontaminated location (VRP9C and VRP9D) fall within the σ' range of samples contaminated with dissolved hydrocarbon (VRP4D and VRP1D). Thus, it is impossible to distinguish contaminated from uncontaminated samples based on the σ' data.

The magnitude of σ'' and ϕ components increases steadily with increasing frequency, and the phase spectra in the contaminated sediments are similar to those observed by Vanhala (1997) in comparable contaminated sediments. Two

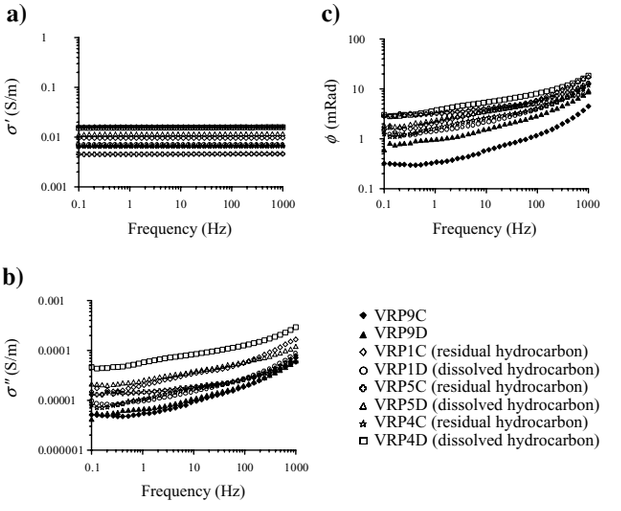

Figure 3. Spectral IP results from the saturated zone over a frequency range 0.1–1000 Hz: (a) real conductivity response σ', (b) imaginary conductivity response σ'', (c) phase response ϕ. Filled black symbols represent uncontaminated locations; unfilled open symbols represent residual and dissolved-phase contamination.

important observations are that (1) the uncontaminated samples (VRP9C and VRP9D) have essentially identical σ'' (Figure 3b) and (2) contaminated samples (residual and dissolved hydrocarbon) clearly show higher σ'' and ϕ magnitudes compared to uncontaminated samples.

The σ', σ'', and ϕ results from the unsaturated zone are shown in Figure 4. Here, the spectra are terminated at 100 Hz because of higher sample resistances; capacitive wiring effects become significant above 100 Hz. Induced-polarization measurements on unsaturated zone samples (Figures 4b, c) exhibit higher σ'' and ϕ magnitudes consistent with measured contaminated samples from the saturated zone (Figures 3b, c). Furthermore, the uncontaminated samples again plot with nearly identical and lower σ''. The σ' and σ'' data from the unsaturated zone (Figures 4a, b) vary more than three orders of magnitude compared to samples from the saturated zone (one order of magnitude) (Figures 3a and 3b, respectively). The ϕ from the unsaturated zone samples (Figure 4c) varies more than two orders of magnitude compared to samples from the saturated zone (one order of magnitude) (Figure 3c). We attribute the broader range of σ' for samples from the unsaturated zone in part to the influence of varying saturation between samples.

Despite the added complexity of variable saturation between samples, clear trends exist between the IP parameters and contamination phase. Most obviously (Figure 4b), there is a clear difference in the σ'' response for samples from the uncontaminated location (filled, black symbols), samples from residual-phase contaminated locations (unfilled, white symbols), and samples from the vadose zone above the residual contamination zone (gray symbols). A similar pattern is observed for the ϕ response, although the distinction between samples located above the zone of residual contamination and samples contaminated with residual hydrocarbon is less obvious. Samples contaminated with residual hydrocarbon (VRP4B, VRP5B, and VRP1B) show the highest σ'' and ϕ magnitudes. Interestingly, samples located above the residual hydrocarbon zone (VRP5A, VRP4A, VRP1A) also show higher σ'' and ϕ magnitudes than uncontaminated samples (VRP9A and VRP9B) from the background location.

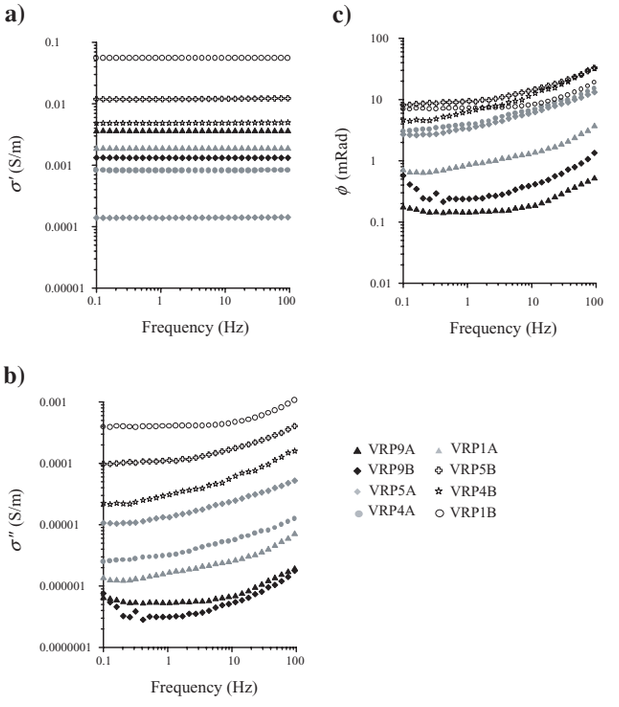

Figure 4. Spectral IP results from the unsaturated zone over a frequency range 0.1–100 Hz: (a) real conductivity response σ', (b) imaginary conductivity response σ'', (c) phase response ϕ. Filled black symbols represent uncontaminated locations; unfilled open symbols represent residual-phase contamination; filled gray symbols represent vadose-zone samples located above residual hydrocarbon contamination.

The σ' and σ'' magnitudes at 1 Hz (close to a typical field IP measurement) are shown as bar plots and are compared with the VRP logs in Figure 5. The plots highlight the high conductivity and polarization observed in the smear zone. The polarization is strongest in the upper (vadose) part of the smear zone (at VRP5B and VRP1B). Werkema et al. (2003) and Atekwana, Werkema et al. (2004) measure highest-bulk conductivities in the vadoze zone immediately above the zone of free-product accumulation and attribute this observation to a region of most intensive microbial degradation.

Figure 6 shows SEM micrographs of five samples representing different zones at the study site (VRP9A, VRP9C, VRP4B, VRP4D, and VRP1B). The SEM micrographs of samples from uncontaminated background locations (VRP9A and VRP9C) show smooth grain surfaces with minimum etch and pit features (Figures 6a, b). However, SEM micrographs of samples representing the hydrocarbon-contaminated zone (VRP4B, VRP4D, and VRP1B) show extensive etching and pitting (Figures 6c–6e, respectively). These micrographs suggest that samples from contaminated locations experience either direct microbial-mineral weathering or mineral dissolution as a result of the production of organic acids and carbonic acids as metabolic byproducts of microbial degradation of hydrocarbon contamination. Furthermore, there is evidence of microbial activity occurring in the unsaturated zone above the residual hydrocarbon region at the contaminated locations (Figure 4b). This supports our notion that biodegradation of vapor-phase contamination may be active at such locations.

Table 2 summarizes the results of nitrogen BET surface-area measurements, porosity estimates, and σ'' at 1 Hz for the same sample set. The surface area-pore volume ratio S_{por} calculated using a mean matrix density of 2.65 g/cm^3 is also tabulated. Contaminated samples (residual and dissolved hydrocarbon) generally exhibit lower S_{por} yet higher σ'' when compared to uncontaminated samples. Two important implications from these observations are that (1) changes in S_{por} do not appear to explain the high σ'' observed for contaminated samples, as σ'' is known to increase near linearly with S_{por} in unconsolidated sediments, and (2) the etching observed with SEM at contaminated locations is not associated with an increase in BET measured surface area.

Control experiments

Figure 7 shows the dependency of σ', σ'', and ϕ at 1 Hz on fluid conductivity σ_w and water saturation S_w in the fine-to-medium sand collected from VRP9 (uncontaminated background location). We used equation 3 to fit σ' at 1 Hz as a

function of σ_w, the effect of σ'_{surf} on σ' being insignificant for the relatively high σ_w range studied here. Figure 7a shows that σ' varies linearly with σ_w over two orders of σ_w magnitude with a formation factor of 6.28 ± 0.21 obtained from least-squares regression (the linear correlation coefficient, or $R^2 = 0.99$). The important observation here is that the IP parameters σ'' and ϕ at 1 Hz are considerably less dependent on σ_w than σ'. The parameter σ'' approximates a power-law σ_w dependence (exponent $= 0.58 \pm 0.03$) within our limited σ_w. These results show close agreement with measurements on similar materials reported elsewhere (Slater and Lesmes, 2002b).

Figure 7b shows that σ'' and ϕ at 1 Hz are also less dependent on water saturation than σ', which varies by two orders of magnitude. Saturation exponents of 1.38 ± 0.02 ($R^2 = 0.99$) and 0.61 ± 0.01 ($R^2 = 0.99$) were obtained from the regression of the σ' and σ'' data, respectively. Our results are again consistent with previous studies (Ulrich and Slater, 2004). A key observation here is that whereas σ_w and S_w impact σ' to a greater extent than they impact σ'', measurements on samples from the field site exhibit greater variation in σ'' than σ'. These control experiments thus suggest that the variability in σ_w and S_w between samples cannot account for our IP observations.

Figure 8 shows the SEM micrographs of the control and treated samples subjected to the mineral-etching procedure of Berner and Holdren (1977). The mineral grains of the control sample (not treated with acid) show a smooth surface with minimal/no etch and pit features (Figure 8a), similar to that observed at uncontaminated locations (Figure 6a). However, samples treated with acids show extensive etching and pitting resulting from mineral grain dissolution (Figures 8b–8e). These mineral surfaces are similar to those observed for the contaminated samples from the field site (Figure 6), suggesting that the formation of etch pits on mineral surfaces of the field samples resulted from acid action.

The results of nitrogen BET surface-area measurements, porosity estimates, and σ'' at 1 Hz obtained for the control and acid-treated samples as a function of time are summarized in Table 3. The surface area-pore volume ratio, calculated using a mean matrix density of 2.65 g/cm^3, is also included in Table 3. The control sample, which was not treated with acid, shows the highest σ'' and S_{por} compared to samples treated with acid. The BET-measured surface area and σ'' both decrease as acid treatment time increases ($\sigma'' \propto S_{por}^{0.65\pm0.07}$; $R^2 = 0.80$). This observation is consistent with a laboratory study showing a reduction in measured BET surface area during acid dissolution of phosphate particles after seven minutes from the start of the experiment (Mgaidi et al., 2003). This result further supports our hypothesis that changes in S_{por} resulting from mineral etching are not responsible for the increase in σ'' at contaminated locations. Thus, changes in the mineral surfaces (etching and pitting) resulting from microbiological activity do not explain the observed IP enhancement.

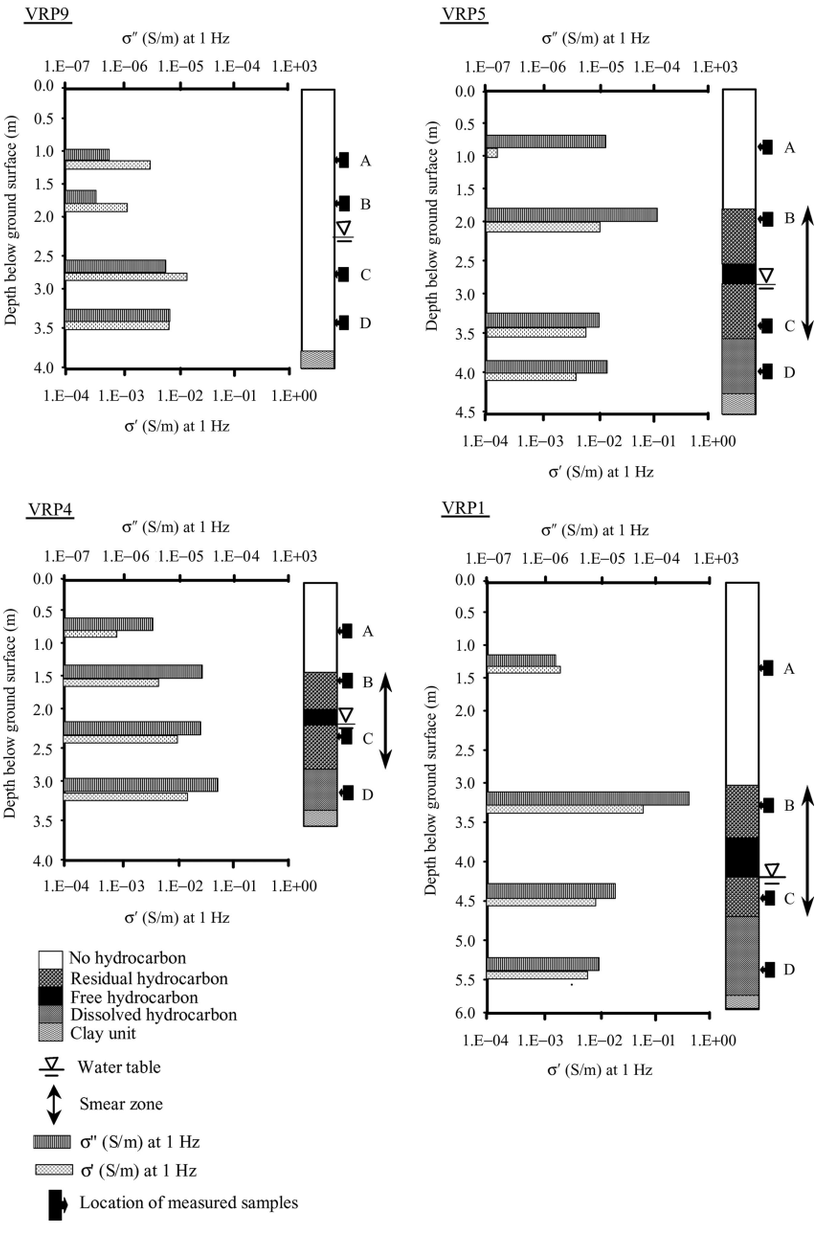

Figure 5. Bar plots of the 1-Hz real (σ') and imaginary (σ'') conductivity. Samples from the unsaturated part of the smear zone (contaminated with residual-phase hydrocarbon) show relatively higher σ' and σ'' magnitudes (except VRP4) compared to dissolved hydrocarbon-contaminated and uncontaminated samples.

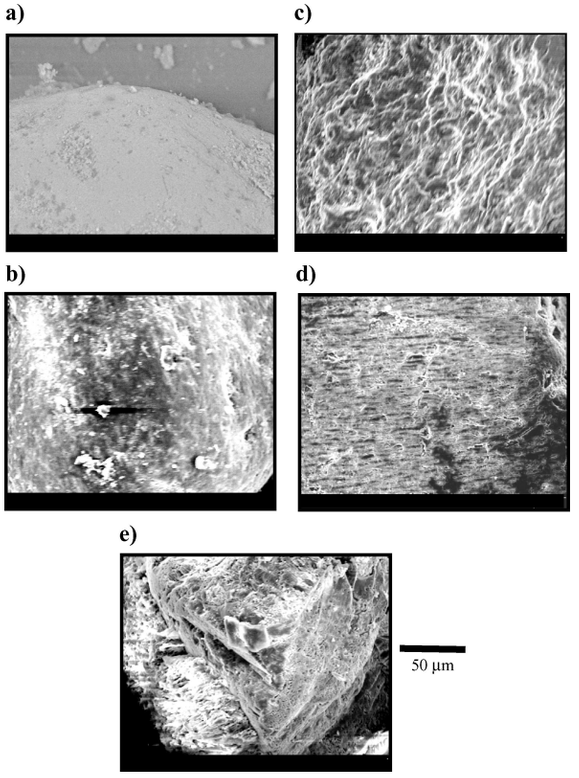

Figure 6. SEM micrographs of five samples representing (a) VRP9A (unsaturated, uncontaminated location), (b) VRP9C (saturated, uncontaminated location), (c) VRP4A (unsaturated, located above residual zone of contamination), (d) VRP4D (saturated, dissolved-contamination zone), and (e) VRP1B (unsaturated, residual-contamination zone). Samples from contaminated locations (VRP4D and VRP1B) show extensive etched pits on mineral surfaces compared to samples from uncontaminated locations (VRP9A, VRP9C, and VRP4A).

DISCUSSION

Microbially induced biophysicochemical changes have the potential to alter electrical signatures at aged hydrocarbon-contaminated sites undergoing biodegradation (Atekwana, Werkema et al., 2004). In our previous laboratory column studies, we demonstrated that biophysicochemical changes over time enhanced both the electrolytic and interfacial electrical properties of unconsolidated sediments undergoing biodegradation (Abdel Aal et al., 2004a, b; Atekwana, Atekwana, Werkema et al., 2004). In this study, we provide evidence indicating that higher magnitudes of IP parameters are coincident with contaminated locations where active biodegradation processes occur. IP parameters (σ'' and ϕ, measured for samples retrieved from the field clearly distinguish between contaminated and uncontaminated samples, these being indistinguishable based on σ' magnitudes (Figures 3 and 4). The contaminated samples are distinguishable from the uncontaminated samples by a relatively higher σ'' magnitude (about two orders). This observation contradicts observations made by Börner et al. (1993) and Vanhala (1997). Their experimental results showed that organic contaminants generally decrease the magnitude of σ''.

We suggest this difference may be the result of variations in maturation time combined with biophysicochemical alterations resulting from biological activity. In the Vanhala (1997) study, although the phase spectra for the clean sand were generally higher and remained stable with time, the magnitude of the phase spectra of oil-contaminated samples increased along with maturation time (several weeks after initial contamination). This implies a shift toward higher ϕ and σ'' with the age of the contamination, consistent with the observations made in this study. Whereas previous investigators used fresh hydrocarbon contaminants, our samples were retrieved from a site where hydrocarbon contamination has existed for more than 50 years and where intrinsic biodegradation of the hydrocarbon was occurring (Atekwana, Atekwana, Legall et al., 2004). Additionally, in the Vanhala (1997) study, samples collected from a hydrocarbon-contaminated field site

Table 2. Measurements of BET surface area, gravimetric porosity, and σ'' at 1 Hz for five samples representing different depth intervals at the study site. The calculated surface area-porosity ratio S_{por} is also shown. Error values were calculated from repeat measurements.

Sample	Zone	Contaminant phase	Porosity	Surface area (m^2/g)	S_{por} μm^{-1}	σ'' at 1 Hz (S/m)
VRP9A	Unsaturated	Uncontaminated (background location)	0.32	1.48	8.15	5.42×10^{-7}
VRP9C	Saturated	Uncontaminated (background location)	0.32	0.24	1.33	5.46×10^{-6}
VRP4A	Unsaturated	Uncontaminated (located above residual contamination zone)	0.28	0.27	1.79	3.21×10^{-6}
VRP4D	Saturated	Dissolved hydrocarbon	0.30	0.74	4.34	5.79×10^{-5}
VRP1B	Unsaturated	Residual hydrocarbon	0.31	0.47	2.65	4.03×10^{-4}
Error			±0.01	±0.05	±0.32	±2%

showed higher phase spectra relative to those of clean samples (Figure 12 of Vanhala, 1997), again consistent with our observations.

So what physicochemical processes cause the hydrocarbon-impacted zone to exhibit higher conductivity and higher magnitudes in the measured IP parameters compared to the uncontaminated zone? The variation in σ_w and S_w between samples is unlikely to explain our IP observations. Control experiments show that σ'' is less dependent than σ' on σ_w and S_w for samples from our field site, consistent with previous studies. In contrast, our samples exhibit a greater range in σ'' than σ'. Furthermore, contaminated samples from the vadose part of the smear zone exhibit the highest σ'' contrary to the power-law dependence of imaginary conductivity on saturation.

SEM micrographs of samples used in this study show that mineral surfaces from the contaminated locations exhibit extensive etching and pitting compared to samples from the background location. This is consistent with studies from other hydrocarbon-contaminated aquifers that have documented etched pits on mineral surfaces and enhanced mineral weathering by microbial colonization of these surfaces (e.g., Hiebert and Bennett, 1992). However, BET measurements show that samples from within the zone of extensive etching and pitting have less surface area compared to uncontaminated samples from the background location (Table 2). Furthermore, the artificial etching experiment shows that dissolution of quartz grains reduces the measured BET surface area and the magnitude of σ'' (Table 3).

The reduction in σ'' in the artificial etching experiment tracks the reduction in BET surface area ($\sigma'' \propto S_{\text{por}}^{0.65\pm0.07}$; $R^2 = 0.80$). The observed decreases in surface area can result from a decrease in mineral surface roughness or from the development of mesoporosity (e.g., Anbeek, 1993; Walker et al., 1995). Mgaidi et al. (2003) describe laboratory studies that show reduction in measured BET surface area during acid dissolution of phosphate particles after seven minutes of etching. Surface area then increases with continued etching. Mgaidi et al. (2003) attribute the initial reduction in surface area to the disappearance of the mineral surface roughness and the subsequent increase to pore widening. Our data reveal an apparent paradox, as the decrease in surface area (Table 2), is inconsistent with the apparent increase in surface roughness as a result of etching and pitting visually observed with SEM (Figures 6 and 8). Furthermore, porosity decreases with acid treatment (Table 3), and porosity is generally lower for samples from contaminated locations (Table 2), even though mineral dissolution is evident. Despite this paradox in our data set, we can draw the following important conclusion from our observations: The enhancement in the σ'' magnitude observed in the contaminated zones cannot be attributed to the mineral etching resulting from biodegradation processes.

The presence of etched pits observed on mineral surfaces from the contaminated locations does, however, provide strong evidence for direct microbial colonization of mineral surfaces (e.g., Hiebert and Bennett, 1992). Microbe-induced mineral weathering and release of ions into solution increases ionic strength of the pore fluids (Bennett et al., 1996), thereby enhancing the attachment of bacteria to soil particles (Maier et al., 2000). Bacteria cells have large surface areas (~30–100 m^2/g) (Van Der Wal, Minor et al., 1997b,c) and high wall counterion charge density (~0.5–1.0 coulombs/m^2)

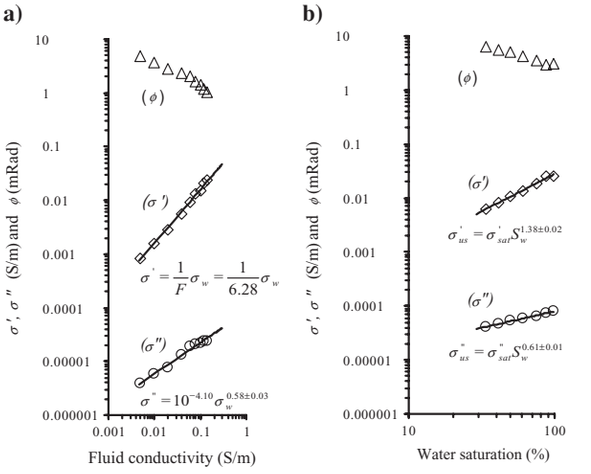

Figure 7. Dependence of the real conductivity σ', imaginary conductivity σ'', and phase response ϕ at 1 Hz on (a) fluid conductivity σ_w and (b) the degree of saturation S_w. The power-law relationships for σ' and σ'' as a function of σ_w and S_w are shown in each case (correlation coefficient, $R^2 > 0.98$ in each case).

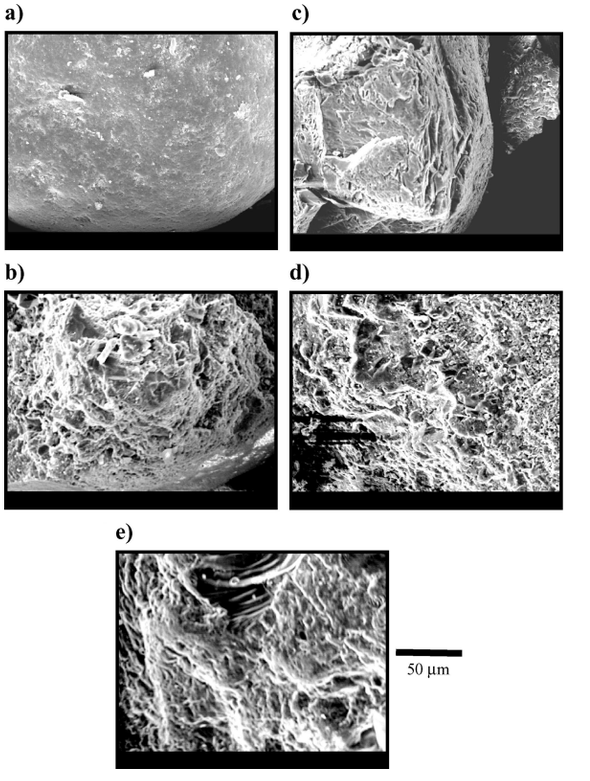

Figure 8. SEM micrographs of sands with and without acid treatment at 20-minute intervals: (a) control sample (no acid treatment), (b) 20-minute acid-treated sample, (c) 40-minute acid-treated sample, (d) 60-minute acid-treated sample, and (e) 80-minute acid-treated sample. Samples treated with acids (b–e) show extensive etched pits on mineral surfaces compared with the untreated sample (a).

(Van Der Wal et al., 1997c). For example, bacterial surface areas are estimated to equal or exceed those of kaolinite (10–22 m^2/g) (Bickmore et al., 2002). Furthermore, the outer membrane of bacterial cells is permeable to ions.

Minerals coated with clays exhibit high-IP effects because of (a) the large surface area of clays (Garrouch and Sharma, 1994; Slater and Lesmes, 2002b) and (b) polarization enhancement when clays block narrow pore throats and generate ion-selective membranes. We suggest that the growth of bacterial cells and their accumulation on the mineral surface (biofilms) similarly enhances interfacial polarization and causes the relatively high-IP response of the contaminated samples compared to uncontaminated samples. Bacterial cells attached to the mineral surface may increase the effective polarizability of the mineral-fluid interface as a result of enhancing surface area and/or charge density. Furthermore, IP enhancement might occur as a result of ion-selective biological membranes forming at pore constrictions, possibly magnified by a geobattery effect (Naudet et al., 2003). Similar effects may result from biodegradation of the vapor-phase hydrocarbon (originating from the residual phase below) in the uppermost part of the vadose zone at contaminated locations. This could explain the relatively higher σ'' and ϕ magnitudes of samples located above the residual hydrocarbon zone (VRP5A, VRP4A, and VRP1A) compared to uncontaminated samples (VRP9A and VRP9B) from the background location at the study site. SEM micrographs show evidence for microbial activity in this zone (Figure 6c) and support this assumption. Further research is clearly needed to investigate the effect of bacterial-cell density and biodegradation of hydrocarbon-vapor phase on IP parameters.

Table 3. Measurements of BET surface area, gravimetric porosity, and σ'' at 1 Hz for sands with and without acid treatment at 20-minute intervals ($\sigma'' \propto S_{por}^{0.65\pm0.07}$, $R^2 = 0.80$). The calculated surface area-porosity ratio (S_{por}) is shown also. Error values were calculated from repeat measurements.

Sample	Acid treatment time (minutes)	Porosity	Surface area	S_{por} (μm^{-1})	σ'' at 1 Hz (S/m)
Control	0	0.36	0.20	0.96	8.71×10^{-6}
1	20	0.35	0.17	0.83	6.03×10^{-6}
2	40	0.36	0.13	0.66	5.18×10^{-6}
3	60	0.35	0.07	0.36	4.57×10^{-6}
4	80	0.34	0.06	0.30	3.25×10^{-6}
Error	±0.5	±0.01	±0.02	±0.12	±2%

On the basis of our results, we offer a simple schematic (Figure 9) of factors impacting electrical properties at hydrocarbon-contaminated sites. Here, we simplify the state of the hydrocarbon-contaminated sediments by categorizing them as either fresh (Figure 9a) or biodegraded (Figure 9b). Initially, a fresh hydrocarbon spill contaminates the sediments and the hydrocarbon displaces water in the pore space (Figure 9a). In addition, hydrocarbons can partition into several phases, including a hydrocarbon fraction sorbed to the mineral grain surfaces (residual phase), dissolved in pore water (dissolved phase), or as a free-floating product (free phase). The presence of fresh hydrocarbons in sediments modifies the electrical signature relative to uncontaminated material. The hydrocarbon-impacted sediments (Figure 9a) show a decrease in electrical conductivity (e.g., De Ryck et al., 1993) and a decrease in the magnitude of the IP response (e.g., Vanhala et al., 1992; Börner et al., 1993; Vanhala, 1997).

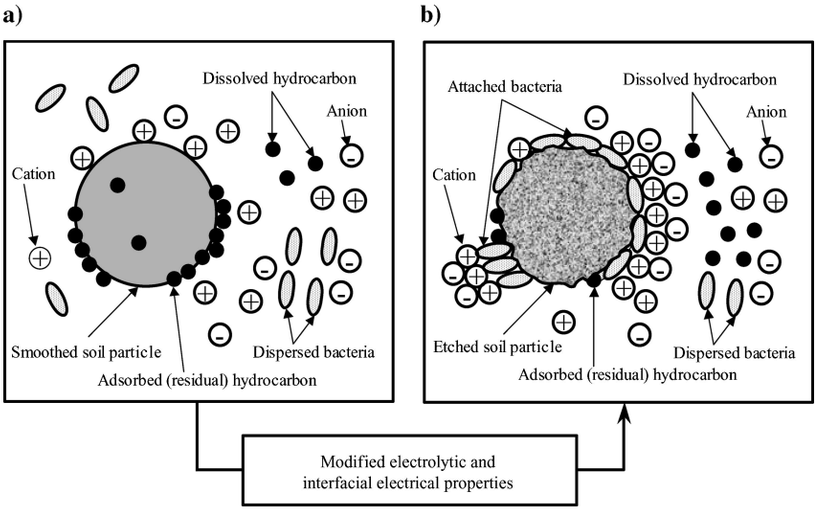

Figure 9. Simple schematic representation of sediment microenvironments at a hydrocarbon-contaminated site. (a) Fresh hydrocarbon-contaminated sediment microenvironment. A fresh hydrocarbon spill is released into the subsurface, replacing the sediment pore water, sorbing to mineral grains and dissolving in the water. (b) Biodegraded-modified microenvironment. Increases in ionic concentration result from the leaching of ions from sediment grains caused by microbial colonization of minerals, dissolution by organic acids produced from hydrocarbon biodegradation, and attachment of charged microbial cells to mineral surfaces. Microenvironment (a) is characterized by low electrical conductivity and IP response, whereas microenvironment (b) is characterized by relatively higher electrical conductivity and IP response.

However, when hydrocarbon-contaminated sediments are modified by biophysicochemical changes induced by microbial degradation of the hydrocarbons, the electrical properties of the subsurface contaminated-environment change. For example, organic acids produced by bacteria enhance mineral weathering and dissolution, releasing ions into solution (Figure 9b). As a result, pore-water conductivity increases and bulk conductivity increases (Atekwana, Werkema et al., 2004; Atekwana, Atekwana, Werkema et al., 2004; Atekwana, Atekwana, Legall, et al., 2004). The increase in pore-fluid ionic strength intensifies the attachment of microbial cells to mineral surfaces (Figure 9b). The accumulation of charged cells in the electrical double layer at the mineral-electrolyte interface, coupled with possible ion transport through cellular membranes blocking pore constrictions, enhance the IP response (Figure 9b) as suggested here and in recent studies (Abdel Aal et al., 2004a, b). Our explanation suggests that IP enhancement begins after the real conductivity enhancement associated with mineral etching and dissolution. Controlled laboratory

column experiments indeed suggest that the first changes in σ' precede changes in σ'' (Abdel Aal et al., 2004b).

CONCLUSION

Hydrocarbon-impacted sites are complex biophysicochemical environments, and intrinsic biodegradation adds more complexity to the geoelectrical properties at these sites. The laboratory results obtained from this study suggest the potential of using IP to investigate hydrocarbon-impacted sites where intrinsic biodegradation occurs. Our results show that the magnitude of the IP response for samples at contaminated locations, particularly in the smear zone, is higher compared to samples from uncontaminated locations, consistent with in-situ resistivity measurements from the site. The high IP magnitude associated with the contaminated samples is most likely related to mineral-fluid or microbial-fluid interfacial electrical properties resulting from microbial activity at the study site. These findings illustrate the potential utility of electrical measurements for noninvasive monitoring of microbial activity at sites undergoing natural hydrocarbon degradation. However, field application of the IP method is necessary to support the laboratory findings and to test the hypothesis of the higher IP magnitude associated with aged hydrocarbon-contaminated sediments.

ACKNOWLEDGMENTS

This work was funded in part by the University of Missouri Research Board and the U. S. Geological Survey (award 000457). We thank Craig Ulrich, Isaiah Utne, and Danney Glaser for their assistance during the preparation of the sample holder and data acquisition. We are grateful to Yuxin Wu (Rutgers University) for making surface-area measurements. Reviews from three anonymous reviewers helped improve this manuscript.

REFERENCES

Abdel Aal, G. Z., E. A. Atekwana, L. D. Slater, and E. A. Atekwana, 2004a, Effect of different phases of diesel biodegradation on low-frequency electrical properties of unconsolidated sediments: Symposium on the Application of Geophysics to Engineering and Environmental Problems (SAGEEP), Proceedings, 386–395.

———, 2004b, Effects of microbial processes on electrolytic and interfacial electrical properties of unconsolidated sediments: Geophysical Research Letters, **31**, L12505, doi:10.1029/2004GL020030.

American Society for Testing and Materials, 2000, Standard practice for classification of soils for engineering purposes (unified soil classification system), designation D2487-00: American Society for Testing and Materials.

Anbeek, C., 1993, The effect of natural weathering on dissolution rates: Geochimica et Cosmochimica Acta, **57**, 4963–4975.

Archie, G. E., 1942, The electrical resistivity log as an aid in determining some reservoir characteristics: Transactions of the American Institute of Mining, Metallurgical and Petroleum Engineers, **146**, 54–62.

Atekwana, E. A., E. A. Atekwana, F. D. Legall, and R. V. Krishnamurthy, 2004, Field evidence for geophysical detection of microbial activity: Geophysical Research Letters, **31**, L23603, doi:10.1029/2004GL021576.

Atekwana, E. A., E. A. Atekwana, R. S. Rowe, D. D. Werkema, and F. D. Legall, 2004, Total dissolved solids in groundwater and its relationship to bulk conductivity of soils contaminated with hydrocarbon: Journal of Applied Geophysics, **56**, 281–294.

Atekwana, E. A., E. A. Atekwana, D. D. Werkema, J. P. Allen, L. A. Smart, J. W. Duris, D. P. Cassidy, W. A. Sauck, and S. Rossbach, 2004, Evidence for microbial enhanced electrical conductivity in hydrocarbon-contaminated sediments: Geophysical Research Letters, **31**, L23501, doi:10.1029/2004GL021359.

Atekwana, E. A., D. D. Werkema, J. W. Duris, S. Rossbach, E. A. Atekwana, W. A. Sauck, D. P. Cassidy, J. Means, and F. D. Legall, 2004, In-situ apparent conductivity measurements and microbial population distribution at a hydrocarbon-contaminated site: Geophysics, **69**, 56–63.

Baker, K. H., and D. S. Herson, 1994, Bioremediation: McGraw-Hill Book Company.

Bennett, P. C., F. K. Hiebert, and W. J. Choi, 1996, Microbial colonization and weathering of silicates in a petroleum-contaminated groundwater: Chemical Geology, **132**, 45–53.

Bermejo, J. L., W. A. Sauck, and E. A. Atekwana, 1997, Geophysical discovery of a new LNAPL plume at the former Wurtsmith AFB, Oscoda, Michigan: Ground Water Monitoring Review, **17**, 131–137.

Berner, R. A., and G. R. Holdren, Jr., 1977, Mechanism of feldspar weathering — II: Observations of feldspar from soils: Geochimica et Cosmochimica Acta, **43**, 1173–1186.

Bickmore, B. R., K. L. Nagy, P. E. Sandlin, and T. S. Crater, 2002, Quantifying surface areas of clays by atomic force microscopy: American Mineralogy, **87**, 780–783.

Börner, F., and J. Schön, 1991, A relation between the quadrature component of electrical conductivity and the specific surface area of sedimentary rocks: The Log Analyst, **32**, 612–613.

Börner, F., M. Gruhne, and J. Schön, 1993, Contamination indications derived from electrical properties in the low frequency range: Geophysical Prospecting, **41**, 83–98.

Bradford, J. H., 2003, GPR offset dependent reflectivity analysis for characterization of a high-conductivity LNAPL plume: Symposium on the Application of Geophysics to Engineering and Environmental Problems (SAGEEP), Proceedings, 238–252.

Brunauer, S., P. H. Emmett, and E. Teller, 1938, Adsorption of gases in multimolecular layers: Journal of the American Chemical Society, **60**, 309–319.

Cassidy, D. P., A. J. Hudak, D. D. Werkema, E. A. Atekwana, S. Rossbach, J. W. Duris, E. A. Atekwana, and W. A. Sauck, 2002, In-situ rhamnolipid production at an abandoned petroleum refinery by *Pseudomonas aeruginosa*: Journal of Soil and Sediment Contamination, **11**, 769–787.

Cassidy, D. P., D. D. Werkema, W. A. Sauck, E. A. Atekwana, S. Rossbach, and J. Duris, 2001, The effects of LNAPL biodegradation products on electrical conductivity measurements: Journal of Environmental and Engineering Geophysics, **6**, 47–52.

Cozzarelli, I. M., M. J. Baedecker, R. P. Eganhouse, and D. F. Goerlitz, 1994, The geochemical evolution of low-molecular-weight organic acids derived from the degradation of petroleum contaminants in groundwater: Geochimica et Cosmochimica Acta, **58**, 863–877.

Cozzarelli, I. M., B. A. Bekins, M. J. Baedecker, G. R. Aiken, R. P. Eganhouse, and M. E. Tuccillo, 2001, Progression of natural attenuation processes at a crude oil spill site: I — Geochemical evolution of the plume: Journal of Contaminanty Hydrology, **53**, 369–385.

Cozzarelli, I. M., J. S. Herman, and M. J. Baedecker, 1995, Fate of microbial metabolites of hydrocarbons in a coastal plain aquifer: The role of electron acceptors: Environmental Science Technology, **29**, 458–469.

DeRyck, S. M., J. D. Redman, and A. P. Annan, 1993, Geophysical monitoring of a controlled kerosene spill: Symposium on the Application of Geophysics to Engineering and Environmental Problems (SAGEEP), Proceedings, 5–20.

Garrouch, A. A., and M. M. Sharma, 1994, The influence of clay content, salinity, stress and wettability on the dielectric properties of brine-saturated rocks: 10 Hz to 10 MHz: Geophysics, **59**, 909–917.

Hiebert, F. K., and P. C. Bennett, 1992, Microbial control of silicate weathering in organic rich ground water: Science, **258**, 278–281.

Knight, R., 1991, Hysteresis in the electrical resistivity of partially saturated sandstones: Geophysics, **56**, 2139–2147.

Legall, F. D., 2002, Geochemical and isotopic characteristics associated with high conductivities in a shallow hydrocarbon-contaminated aquifer: Ph.D. dissertation, Western Michigan University.

Lesmes, D. P., and K. M. Frye, 2001, Influence of pore fluid chemistry on the complex conductivity and induced-polarization responses of Berea Sandstone: Journal of Geophysical Research, **106**, no. B3, 4079–4090.

Lima, O. A. L., and S. Niwas, 2000, Estimation of hydraulic parameters of shaly sandstone aquifers from geoelectrical measurements: Journal of Hydrology, **235**, 2–26.

Longeron, D. G., M. J. Argaud, and J. P. Feraud, 1989, Effect of overburden pressure and the nature and microscopic distribution of

fluids on electrical properties of rock samples: Society of Petroleum Engineers Formation Evaluation, **4**, 194–201.
Maier, R. M., I. L. Pepper, and C. P. Gerba, 2000, Environmental microbiology: Academic Press.
Mgaidi, A., F. B. Brahim, D. Oulahna, M. El Maaoui, and J. A. Dodds, 2003, Change in surface area and dissolution rate during acid leaching of phosphate at 25°C: Industrial and Engineering Chemistry Research, **42**, 2067–2073.
Naudet, V., A. Revil, J. Y. Bottero, and P. Bégassat, 2003, Relationship between self-potential (SP) signals and redox conditions in contaminated groundwater: Geophysical Research Letters, **30**, 2091, doi:10.1029/2003GL018096.
Park, D. H., and J. G. Zeikus, 2000, Electricity generation in microbial fuel cells using neutral red as an electronophore: Applied Environmental Microbiology, **66**, 1292–1297.
Pasteris, G., D. Werner, K. Kaufmann, and P. Hohener, 2002, Vapor phase transport and biodegradation of volatile fuel compounds in the unsaturated zone: A large scale lysimeter experiment: Environmental and Scientific Technology, **36**, 30–39.
Redman, J. A., S. Walker, and M. Elimelech, 2004, Bacterial adhesion and transport in porous media: Role of the secondary energy minimum: Environmental and Scientific Technology, **38**, 1777–1785.
Revil, A., and P. W. J. Glover, 1998, Nature of surface electrical conductivity in natural sands, sandstones, and clays: Geophysical Research Letters, **25**, 691–694.
Ron, E. Z., and E. Rosenberg, 2001, Natural roles of biosurfactants: Environmental Microbiology, **3**, 229–336.
Sauck, W. A., 2000, A conceptual model for the geoelectrical response of LNAPL plumes in granular sediments: Journal of Applied Geophysics, **44**, 151–165.
Sauck, W. A., E. A. Atekwana, and M. S. Nash, 1998, Elevated conductivities associated with an LNAPL plume imaged by integrated geophysical techniques: Journal of Environmental and Engineering Geophysics, **2**, 203–212.
Schön, J. H., 1996, Physical properties of rocks — Fundamentals and principles of petrophysics: Pergamon Press.
Slater, L., and D. Glaser, 2003, Controls on induced-polarization in sandy unconsolidated sediments and application to aquifer characterization: Geophysics, **68**, 1547–1558.
Slater, L., and D. P. Lesmes, 2002a, Electrical-hydraulic relationships observed for unconsolidated sediments: Water Resources Research, **38**, 1213, doi: 10.1029/2001WR001075.
———, 2002b, IP interpretation in environmental investigations: Geophysics, **67**, 77–88.
Ulrich, C., and L. Slater, 2004, Induced-polarization measurements on unsaturated, unconsolidated sands: Geophysics, **69**, 762–771.
Van Der Wal, A., M. Minor, W. Norde, A. J. B. Zehnder, and J. Lylkema, 1997a, Conductivity and dielectric dispersion of gram-positive bacterial cells: Journal of Colloid and Interface Science, **186**, 71–79.
———, 1997b, Determination of the total charge in the cell walls of gram-positive bacteria: Colloids and surfaces B: Biointerfaces, **9**, 81–100.
———, 1997c, Electrokinetic potential of bacterial cells: Langmuir, **13**, 165–271.
Vanhala, H., 1997, Mapping oil-contaminated sand and till with the spectral induced-polarization (SIP) method: Geophysical Prospecting, **45**, 303–326.
Vanhala, H., H. Soininen, and I. Kukkonen, 1992, Detecting organic chemical contaminants by spectral-induced-polarization method in glacial till environment: Geophysics, **57**, 1014–1017.
Vinegar, H. J., and M. H. Waxman, 1984, Induced-polarization of shaly sands: Geophysics, **49**, 1267–1287.
Volkering, F., A. M. Breure, and W. H. Rulkens, 1998, Microbiological aspects of surfactant use for biological soil remediation: Biodegradation, **8**, 401–417.
Walker, F. D. L., M. R. Lee, and I. Parsons, 1995, Micropores and micropermeable texture in alkali feldspars: geochemical and geophysical implications: Mineralogical Magazine, **59**, 505–534.
Waxman, M. H., and L. J. M. Smits, 1968, Electrical conductivities in oil-bearing shaly sands: SPE Journal, **243**, 107–122.
Werkema, D. D., E. A. Atekwana, A. Enders, W. A. Sauck, and D. P. Cassidy, 2003, Investigating the geoelectrical response of hydrocarbon contamination undergoing biodegradation: Geophysical Research Letters, **30**, 1647, doi:10.1029/2003GL017346.